UNITED STATES DEPARTMENT OF THE INTERIOR

GEOLOGICAL SURVEY

The Gladiator Mine, Lake City, Colorado: The mineralogy and paragenesis of an epithermal base- and precious-metal vein system

By

Dana J. Bove[1]

Open-File Report 87-489

1987

[1]Denver, Colorado

CONTENTS

ILLUSTRATIONS

TABLES

ABSTRACT

A fissure-filling epithermal vein, which is exposed in the Gladiator mine, Lake City, Colorado, is similar in size and mineralogy to many other veins in the area. The vein mineralogy of this nonproducing mine is dominated by common epithermal base-metal and gangue minerals. Silver, which is the most abundant precious metal in the vein, occurring in concentrations up to 500 ppm in selected samples, is present in tetrahedrite and rare acanthite. Although gold was detectable in trace amounts (1-10 ppm) by analytical techniques, no Au or Au-bearing minerals were observed in hand specimen or petrographically. Three principal stages of mineralization were differentiated in the vein exposed in the Gladiator mine. From oldest to youngest these include: I quartz-sericite-pyrite; IIa sphalerite-galena, IIb Cu-sulfide; IIIa quartz-barite-rhodochrosite, and IIIb late barite-quartz. In general, each of these assemblages is paragenetically distinct; however, some overlapping of individual minerals within assemblages is common. Six primary fluid inclusions from stage I quartz were measured by R.F. Sanford (unpublished data). Homogenization temperatures ranged from 189.6-224.5°C and averaged 208°C. These temperatures are at the low end of the range for fluid inclusions from the Lake City area.

INTRODUCTION

The Lake mining district (Irving and Bancroft, 1911) contains some of the more prominent mines in the Lake City, Colorado area including the Gladiator mine-the topic of this report-as well as the Golden Fleece, Black Crook, and Golden Wonder mines (fig. 1). Production from mines in the Lake mining district, exclusive of the Gladiator mine, has amounted to about $1.5 million, most of which was recovered between 1890 and 1903 (Irving and Bancroft, 1911). The Golden Fleece mine, which is noted for its occurrence of interbanded uraninite and Au-and-Ag tellurides (Grauch and others, 1985), accounted for over $1.4 million of this production.

The Gladiator mine, which is located approximately 5 km southeast of Lake City, in the eastern portion of the 29 m.y. Uncompahgre caldera (fig. 1), was chosen for a separate detailed mineralogic and geochemical investigations because all underground workings were accessible at the time of study. Inasmuch as production for the Gladiator mine was not recorded in historical mining records (Norma Swanson, oral commun., 1985) or in the comprehensive report on the mines of the Lake City area by Irving and Bancroft (1911), it is assumed that no significant ore production occurred from the Gladiator Mine. In a letter written in 1901 by Gladiator mine superintendent Thomas A. Dall, hand-sorted vein samples were reported to average 0.20 oz Au/ton and 0.40 oz Ag/ton; whereas assays from nine hand- picked dump samples were said to average 0.16 oz Au/ton and 0.20 oz Ag/ton. The same records state that the Gladiator mine was patented in 1881 and was active, probably as an exploratory venture, between 1897 and 1901. Recent mining activity by the Colorado Gold and Silver Company took place between 1980 and 1982; however no ore production was recorded during this time as well. From 1982 to the present the mine has been inactive.

The purpose of this report is to present detailed geologic, mineralogic, and paragenetic data for the vein exposed in the Gladiator mine. These data, when integrated with similar data from other veins in the Lake City area can be used to constrain the timing of geologic and hydrothermal events associated with development of the Lake City caldera, and to understand the evolution of a caldera system from the time of initial magma emplacement, through caldera

formation, to the initiation of a circulating hydrothermal system and the precipitation of base and precious metals.

GEOLOGY AND MINE WORKINGS

The stratigraphy, structure, and petrology of the western San Juan region and the Lake City area are discussed by Lipman and others (1973, 1976), Lipman (1976a and 1976b), Steven and Lipman (1976), and Hon (unpublished data). Geophysical work by Grauch and others (1985; 1987) has defined the subsurface extent of several intrusive bodies whose relationship with hydrothermal veins is currently being investigated. Reynolds and others (1983; 1986) showed that Lake City caldera events spanned the time of one paleomagnetic reversal, about 300,000 years. Lipman and others (1976) and Grauch and others (1985) have discussed multiple events of mineralization in the area; and Bove (1984; 1987; and unpublished data) has studied the alunite deposit on Red Mountain. R.F. Sanford (1985; 1987) is conducting studies on the mineralogy, geochemistry, fluid inclusions, and ages of the veins in the Lake City area.

Veins from the western San Juan mountains range in age from about 10-30 m.y. (Slack and Lipman, 1976). The only dated veins from the Lake City area are the Golden Fleece at 27.5 m.y. (Hon and others, 1985) and the Ute-Ulay, dated at 21.8 m.y. (Slack, 1976). Presently, sericite[1] separates from the Gladiator vein are being collected for Ar^{40}-Ar^{39} dating; however, geologic data constrains the age of the Gladiator vein at less than 29 m.y., the approximate age of the host rocks, although it could be as young as 10 m.y. (Slack and Lipman, 1976).

The Gladiator vein occurs primarily in biotite-quartz latite rocks in the Burns Member of the Silverton Volcanics (Lipman, 1976); these are made up of post-caldera collapse lava flows and domes emplaced along the eastern margin of the 29-m.y.-old Uncompahgre caldera.

The main workings of the Gladiator mine are located at an elevation of 9,060 ft, approximately 60 ft above and to the west of the road to Lake San Cristobal. A detailed map of the Gladiator mine was published in Kirk and others (1983). A generalized map of the mine is shown in figure 2.

The Gladiator mine is comprised of three working levels (fig. 3) with over 500 meters of tunnels. Although all three tunnels were initially driven along the northeast-trending Gladiator vein, nearly 100 meters of the main level drift was tunneled through relatively unmineralized rock. Apparently, the miners were searching for the western continuation of the Gladiator vein, which was offset by a strong northwest-trending fault. Immediately west of the offsetting fault, a cross-cut extending nearly 17 meters to the south intersects what may be either the offset portion of the Gladiator vein, or a parallel but similarly mineralized vein; mine workers named this structure the "David vein". Tunnels along the anastomosing "David vein" extend a maximum distance of 35 meters to the west before terminating; branches of this vein appear in the backs of these tunnels indicating that the vein probably continues to the west. Another northeast-trending vein is intersected near the end of the main tunnel; a projection of this structure could either link up to the Gladiator or the "David vein".

The strike of the Gladiator vein remains fairly consistent on all three levels and averages N35-45^{o}E with relatively steep dips of 75-85^{o}. Commonly widening and thinning, the vein width varies from 10-15cm's up to 1.5 meters and typically widens and horsetails at the intersections of stronger cross fractures. Wider sections of the vein are commonly stoped with some stoped zones continuing nearly 23 meters along strike and extending vertically 3-15

meters. Several ore chutes were recently installed by the Colorado Gold and Silver Company along some of the wider stoped areas; these chutes are located along the first few hundred feet of drift on the main level.

MINERALOGY AND PARAGENESIS

Three principal mineral assemblages are differentiated within the Gladiator vein; these assemblages also coincide with paragenetic stages. From oldest to youngest these paragenetic stages are I quartz-sericite-pyrite (Q-S-P); IIa sphalerite-galena (S-G), IIb Copper-sulfide (Cu-S); IIIa, quartz-barite- rhodochrosite (Q-B-R), and IIIb late barite-quartz (LB-Q). Figure 4 depicts the generalized paragenesis for the Gladiator mine; the individual stages along with their component minerals are listed in table 1. Each assemblage is usually distinguishable in hand specimen. As shown in figure 5, mineralization typically proceeded from the fissure walls inward (from stage I-III) and formed a crude sequence of banding. Only minor fracturing occurred between vein stages and no brecciation of mineral stages was observed.

Division of the three main mineral assemblages is based on the following criteria: (1) recurrent mineral associations, (2) consistent paragenetic relations between recurrent mineral groups based mostly on the observation of cross-cutting, vein-filling, or encrusting relationships, and (3) the differentiability of the main stages in hand samples. Although the principal mineral assemblages are easily recognized megascopically, crosscutting relationships are predominately observed in thin sections. According to the above-mentioned guidelines established for stage separation, both stages II and III have been subdivided. Stage II was divided because assemblages IIa (S-G) and IIb (Cu-S) were separable only under the microscope. On the other hand, there were not enough clear-cut relationships between the Q-B-R (IIIa) and LB-Q (IIIb) assemblages to warrant their separation into two main stages; therefore, these assemblages were incorporated as substages within stage III.

In general, each stage is paragenetically distinct and characterized by a predominance of the minerals defining that assemblage; however, overlapping of stages or individual minerals within them is common.

More than 15 primary sulfides, gangue minerals, and secondary minerals have been identified by detailed petrographic, X-ray diffraction, and electron microprobe analysis. The primary sulfides, which occur predominately as filling veins, in order of decreasing abundance include pyrite, sphalerite, galena, chalcopyrite, tetrahedrite-tennantite, Ag-bearing tetrahedrite, marcasite, and acanthite. Principal gangue minerals are quartz, which comprises most of the vein and much of the Q-S-P altered wallrock, barite, rhodochrosite, and sericite. Hematite, jarosite, limonite, covellite, and chrysocolla comprise the secondary vein minerals and were probably formed by oxidation of main stage sulfide minerals. Although these secondary minerals occur throughout the Gladiator mine, they are volumetrically insignificant.

STAGE I (Q-S-P)

Equigranular mosaics of fluid inclusion-rich quartz, sub-euhedral aggregates of pyrite, sericite, and tiny inclusions of tetrahedrite, tennantite, and rare acanthite define the Q-S-P assemblage (stage I). These minerals occur as vein fillings and/or disseminations in altered wallrock.

Stage I (Q-S-P) vein-quartz is light-medium gray to milky white in hand specimen and typically forms equigranular mosaics of subhedral-euhedral crystals averaging 0.1-0.2 mm in width. In general, early quartz is intimately associated with early pyrite and sericite. In thin section, stage

I (Q-S-P) quartz is distinctively dirty or turbid in appearance due to the presence of abundant fluid inclusions.

Stage I pyrite occurs mainly within the vein and as fine disseminations in altered wallrock. In the Q-S-P assemblage, there is a direct correlation between the abundance of pyrite and its morphology. Where less prevalent, pyrite usually consists of discrete euhedral cubes averaging 0.1-0.2 mm, although occasionally it occurs in clusters of several interlocking, subhedral-euhedral grains. As the volume of pyrite increases, it more typically is observed as clots of adjoining subhedral-euhedral grains with anhedral-subhedral aggregate margins. Stage I (Q-S-P) pyrite grains commonly show polygonal zoning as evidenced by regular planes of pits and inclusions as well as by distinct changes in texture and polishing properties. Tiny inclusions (10-12 microns in width) of near end-member tennantite, and rare tetrahedrite and copper-bearing acanthite, occur as tiny rounded blebs in stage 1 pyrite.

Sericite, identified by X-ray diffraction as the 1M polytype, occurs predominately in altered wallrock adjacent to the vein, and less commonly within the vein. Vein sericite typically occurs as fine-grained wisps and disseminations associated with stage I (Q-S-P) quartz and pyrite. In several samples, sericite forms as fine-grained radiating masses. Sericite is conspicuously absent within later stages (II and III) of barite and quartz.

Fluid inclusion-rich quartz was the first phase crystallized within the stage I assemblage. It is accompanied and is followed by pyrite and sericite crystallization. Some tetrahedrite, tennantite and minor acanthite crystallized prior to pyrite as evidenced by blebs of these minerals included within early pyrite. Pyrite, which characteristically formed around early, sub-euhedral, fluid inclusion-rich quartz grains, commonly contains tiny inclusions of sericite. Sericite is typically observed at the interface between fluid inclusion-rich quartz and early stages of quartz overgrowth. Probably coprecipitated with early pyrite, sericite embays or replaces early fluid inclusion-rich quartz and occurs as inclusions along fracture surfaces within stage I (Q-S-P) pyrite.

Galena, sphalerite, tetrahedrite-tennantite, and chalcopyrite reside along intergranular margins, fractures, cleavage planes, and zone boundaries in early pyrite. These pyrite-hosted sulfides occur along two kinds of planes. The first, as seen in figure 10, plane A, is continuous and delineates fractures, intergranular margins, and overgrowth boundaries. Sulfides occurring along these surfaces clearly post-date the pyrite host. The other type of surface is discontinuous and in thin section appears as rows of sulfide inclusions as illustrated in figure 6, plane B. Etching in a solution of $KMnO_4$-H_2SO_4 reveals that some of the discontinuous planes represent grain margins and zone or overgrowth margins. It is speculated that many of the more linear, discontinuous surfaces represent cleavage planes or microfractures. As shown in figure 6, plane C, both the continuous and discontinuous surfaces commonly link, suggesting that they are the same generation and represent a replacement feature along these surfaces. These sulfides replacing stage I pyrite occur principally in stages IIa (S-G) and IIb (Cu-S), and will be disscussed in the following pages.

STAGE IIa (S-G)

Crystallization of sphalerite, galena, quartz, barite, and minor pyrite occured during stage IIa.

Galena is mostly in assemblage IIa (S-G); however, some overlap occurs with stage IIb (Cu-sulfide) tetrahedrite. Early crystallized galena (stage IIa) formed as subhedral-euhedral, equant crystals averaging between 0.2-1 mm in width, and as illustrated in figure 7 are commonly enveloped by anhedral-subhedral sphalerite. In a number of thin sections, these early galena crystals are deeply embayed and replaced by sphalerite, commonly leaving isolated, irregular islands of optically oriented galena enveloped in a matrix of anhedral to subhedral sphalerite (fig. 8). Less commonly, galena occurs as small, anhedral masses that encrust or surround the earliest generation of galena as well as the enveloping sphalerite. In turn, minor amounts of anhedral sphalerite surround this later crystallized galena.

Galena commonly surrounds, embays, and cross-cuts Stage I (Q-S-P) pyrite. In addition, euhedral grains of stage I (Q-S-P) pyrite crystals are locally included within single crystals of early stage IIa (S-G) coarse-grained galena.

Sphalerite, which occurs almost entirely in stage IIa (S-G) crystallized as anhedral-subhedral masses that average 1-3 mm in diameter and are characterized by complex patterns of color zoning and parallel-subparallel bands of overgrowth. Growth zones within sphalerite are distinctly colored, and small scale, irregular color bands within individual growth zones are observed. Typically, sphalerite is translucent in transmitted light with colors ranging from very light brown to almost clear, yellowish brown, red brown, and green. For the most part, no consistent paragenetic sequence of color zoning has been observed; however, when present, bands of green sphalerite consistently postdate all other sphalerite. Semiquantitative electron microprobe analysis revealed no gross differences in the zinc, sulfur, or iron contents of the sphalerite in different colored zones and bands; however, within homogeneously colored bands or growth zones, iron concentrations varied, although no obvious patterns or zones emerged. Inclusions of other sulfides are uncommon within sphalerite; however, pyrite was periodically precipitated with sphalerite as evidenced by rare inclusions of pyrite within growth zones in the sphalerite.

Fluid inclusion-rich stage I quartz grains are commonly overgrown by "clean" quartz with successive generations of overgrowth delineated by thin "dirty" or fluid inclusion-rich bands. Quartz overgrowth crystallization occurred during stage IIa (S-G) and continued late into the vein paragenesis and typically culminated in the precipitation of medium-coarse grained, euhedral prisms that grew into open space (discussed in sections on later stages). In many instances, this late vug-filling quartz formed interstitial fillings around other late-formed, vug-lining crystals.

Similar to quartz, barite also episodically spans the crystallization history of the vein. Within stage IIa (S-G), barite is characteristically milky white in hand sample and forms subhedral to euhedral, lath-shaped crystals that are interstitially filled in many samples by clean quartz (lacking fluid inclusions) and sulfides. In this stage, barite is extremely variable in size ranging from 0.1-0.2mm up to 1-2 cm in length.

Clearly post-dating stage I (Q-S-P) pyrite and fluid inclusion-rich quartz, galena and sphalerite mineralization occurred during or soon after an early pulse of fluid inclusion-poor quartz overgrowth. Although a few relationships between galena and sphalerite are paragenetically unclear, most thin section evidence supports the interpretation that these minerals formed in a sequence of alternating crystallization. As shown in figures 7 and 8, the onset of galena precipitation probably preceded that of sphalerite, with

alternating episodes of sphalerite and galena crystallization following. In this major episode of alternating sphalerite-galena crystallization, galena typically was the last precipitated mineral. This is substantiated by the presence of late galena either intergrown with later precipitated tetrahedrite (stage IIb) or galena occurring within fractures that cut sphalerite.

Barite, which crystallized early in stage IIa initially developed in open space. In general, barite nucleated from the vug-lining walls of stage I (Q-S-P) minerals, although in some instances it formed from the surfaces of both stage I (Q-S-P) minerals and early generations of stage IIa (S-G) sphalerite; in turn, stage IIa (S-G) barite crystals were interstitially filled by later generations of stage IIa (S-G) sphalerite (sometimes differently colored), galena, quartz, as well as stage III (Q-B-R, LB-Q) minerals.

STAGE IIb (Cu-S)

Stage IIb (Cu-S) is defined by the presence of chalcopyrite, fine-grained pyrite, tetrahedrite, and Ag-bearing tetrahedrite. In general, these minerals occur either alone or as interpenetrating crystal aggregates that commonly surround stage IIa (S-G) galena and sphalerite. In the Gladiator mine, stage IIb (Cu-S) minerals comprise the majority of the fracture-filling sulfides that commonly cross-cut earlier formed sulfide phases.

Chalcopyrite, one of the principal diagnostic minerals of stage IIb (Cu-S), is sparse to moderately abundant in the Gladiator mine. Although almost exclusively allotriomorphic in habit, it was also observed as subhedral crystals in cavities. Chalcopyrite commonly forms the matrix between late (post-stage I), fine-grained pyrite and tetrahedrite (stage IIb); typically these three minerals surround masses of stage IIa (S-G) galena and sphalerite. In the absence of other sulfides, chalcopyrite commonly occurs in voids and between adjacent, subhedral-euhedral quartz gangue. In addition to being one of the most common fracture-filling sulfides, chalcopyrite characteristically occurs as thin intergranular films (fig. 9) that crystallized along grain boundaries between earlier formed sulfides as well as gangue minerals. As seen in figure 10, chalcopyrite that penetrated along sulfide grain boundaries, locally interconnects with fractures filled with chalcopyrite.

Stage I (Q-S-P) pyrite is commonly overgrown and interstitially filled by later stages of relatively finer grained pyrite. Grouped mostly in stage IIb (Cu-S), this later fine-grained pyrite is frequently observed and occurs as subhedral grains ranging from 0.02-0.06mm in diameter. Although also characteristically associated with both chalcopyrite and tetrahedrite, stage IIb (Cu-S) fine-grained pyrite in some samples occurs exclusively within anhedral masses of tetrahedrite.

The tetrahedrite group minerals, although less abundant than galena, sphalerite, and chalcopyrite, are common in the mine. Compositionally, the tetrahedrite mineral group includes near end-member tetrahedrite, Ag-bearing tetrahedrite, and arsenic-bearing, antimony-rich tetrahedrite; however, near end-member tetrahedrite and silver-bearing tetrahedrite are the dominant stage IIb (Cu-S) sulfosalts. Tetrahedrite along with silver- bearing tetrahedrite comprise the majority of stage IIb (Cu-S) sulfosalts; these two minerals are generally in close spatial association with chalcopyrite and stage IIb (Cu-S) fine-grained pyrite. In addition to forming fine-medium grained, allotriomorphic masses that surround most earlier formed sulfides, tetrahedrite and silver-bearing tetrahedrite occur as intergranular films and fracture fillings between and within these older sulfides. Similar to

chalcopyrite, thin intergranular films of these mineral sometimes interconnect with tetrahedrite and/or chalcopyrite-filled fractures which cut across the marginally rimmed pre-stage IIb (Cu-S) sulfide grains.

Preliminary electron microprobe reconnaissance indicates that tetrahedrite-tennantite minerals contain small amounts of zinc. In addition, silver, which is present most commonly in near end-member tetrahedrite, rarely occurs in arsenic-bearing, antimony-rich tetrahedrite.

Comtemporaneity of stage IIb (Cu-S) sulfides is evidenced by the following common intergrowth textures: (1) subhedral-euhedral finely disseminated pyrite occurring exclusively in an anhedral matrix of tetrahedrite (fig. 11), and (2) anhedral masses of mutually interpenetrating chalcopyrite and tetrahedrite. Fracture-filling, overgrowth, and encrusting relations as discussed above indicate the post stage I (Q-S-P) and IIa (S-G) paragenetic positioning of stage IIb sulfides. Chalcopyrite and less commonly tetrahedrite occur as thin intergranular bands or films along grain boundaries between both sulfides and gangue minerals. As illustrated in figure 10, these thin intergranular films of these mineral locally interconnect with chalcopyrite-or tetrahedrite-filled fractures which cut across the marginally rimmed sulfide grains. In some instances chalcopyrite precipitated between adjacent grains of tetrahedrite and early generations of stage IIIa (Q-B-R) rhodochrosite; this relationship indicates that chalcopyrite crystallization continued late into stage IIb (Cu-S) and in part overlapped with early mineralization in stage IIIa (Q-B-R).

STAGE IIIa (Q-B-R)

Stage IIIa (Q-B-R) is defined by the presence of quartz, barite, and rhodochrosite. These minerals occur locally in vugs and within the central open portions of the veins.

Rhodochrosite, like barite, is unevenly distributed throughout the vein, and where present varies from sparse to abundant. Rhodochrosite is typically pink to pinkish-white in hand sample and forms sub-euhedral, tabular to rhomb-shaped crystals, which vary considerably in size. Multiple episodes of rhodochrosite mineralization took place in stage IIIa (Q-B-R); this is evidenced by (1) sequential growth bands of rhodochrosite included within quartz overgrowths; (2) relatively coarse-grained, subhedral-euhedral rhodochrosite rimmed by optically discontinuous, fine-grained rhodochrosite; and (3) coarse masses of rhodochrosite that upon closer inspection show different generations of rhodochrosite distinguished by changes in color, birefringence, grain size, and texture.

Semiquantitative microprobe studies indicate that rhodochrosite contains cations including iron and minor calcium substituting for manganese. Microprobe traverses across different generations of rhodochrosite revealed no significant fluctuations in these elements. Although typically subhedral-euhedral, several samples contain thin, nearly continuous bands composed of colloform or spherical masses (1-4 mm in width) of microcrystalline rhodochrosite. In thin section, these individual rhodochrosite masses are radial or spherical in appearance with thin, closely spaced, sub-parallel growth bands. These microcrystalline masses of rhodochrosite typically nucleated from coarse-grained, rhodochrosite (early stage IIIa) or from stage II (S-G, Cu-S) mineral masses. In turn, bands of microcrystalline rhodochrosite are encrusted by thin bands of quartz. The quartz bands are commonly encrusted by stage IIIb (LB-Q) barite.

Fine-grained pyrite is commonly disseminated in early generations of stage IIIa (Q-B-R) rhodochrosite; in addition, it is often included in discrete bands in stage IIIa (Q-B-R) quartz overgrowths.

Within staged IIIa, barite is characteristically milky white in hand specimen and forms subhedral-euhedral, lath-shaped crystals. Stage IIIa barite crystals are extremely variable in size ranging from 0.1-0.2 mm up to 1-2 cm in length. Crystal interstices in many samples are filled by clean quartz and sulfides.

Although minerals within stage IIb (Cu-S) generally pre-date phases within the Q-B-R assemblage (IIIa), some overlapping of these stages occurs. Some examples of overlap are (1) rare grains of anhedral to nearly botryoidal, fine-grained pyrite, tetrahedrite, and chalcopyrite which lined the euhedral crystal terminations of early crystallized rhodochrosite, (2) finely disseminated pyrite intergrown with early rhodochrosite, (3) thin bands of fine-grained pyrite included along growth planes in stage IIIa (Q-B-R) quartz, and (4) chalcopyrite occurring in fractures and along grain margins within and between early generations of rhodochrosite.

Rhodochrosite, which crystallized episodically throughout stage IIIa (Q-B-R), nucleated from the surfaces of stage II (S-G, Cu-S) sulfides. Early generations of rhodochrosite typically contain inclusions of fine-grained pyrite and sparse chalcopyrite, whereas these sulfides diminish or are nonexistent in later crystallized rhodochrosite. Stage IIIa (Q-B-R) rhodochrosite and barite may have formed cogenetically as suggested by mutually interpenetrating crystal faces and alternating paragenetic relations.

Similar to rhodochrosite, quartz precipitation appears to have spanned stage IIIa (Q-B-R) mineralization. As mentioned previously, bands of rhodochrosite and (or) pyrite are included in stage IIIa (Q-B-R) quartz, apparently delineating successive stages of quartz overgrowth. In addition, stage IIIa (Q-B-R) quartz has formed around and interstitial to vug-filled barite and rhodochrosite.

STAGE IIIb (LB-Q)

Assemblage IIIb (LB-Q) is characterized by barite, quartz, marcasite, and pyrite.

Stage IIIb quartz is composed chiefly of fine, milky colored, euhedral grains; however, bands of blue-gray chalcedonic quartz averaging 1-2mm in width occur sporadically throughout the Gladiator mine. Where present, these bands typically contain minute interlayers of fine-grained marcasite and pyrite.

When present, stage IIIb (LB-Q) barite along with quartz and minor iron-sulfides comprise the central open portion of the vein. In comparison to the previous stages, stage IIIb (LB-Q) barite is relatively clear to slightly honey colored and forms euhedral, lath-shaped crystals averaging 4-5 mm in width. Stage IIIb (LB-Q) barite crystals always occur in open space and grew from the surfaces of thin bands of stage IIIb chalcedonic quartz. Several samples display quartz boxwork which probably originated from the dissolution of barite and later infilling of barite casts by quartz.

Marcasite is a relatively minor phase and occurs exclusively in the late barite-quartz assemblage (stage IIIb). Marcasite formed fine-grained, euhedral, tabular-elongate to rectangular-shaped crystals that are commonly surrounded by later generations of pyrite that mimic the euhedral marcasite morphologies; generally, either one or both iron-disulfides are enclosed within a later generation of botryoidal pyrite. Marcasite and pyrite

generally occur as paper-thin seams within narrow bands of late blue-gray chalcedonic quartz. Although marcasite is relatively minor and fine-grained, it is unusually abundant in one sample with crystals ranging up to 0.2 mm in width and 0.6 mm in length.

Stage IIIb vug-filling minerals, which nucleated from stage IIIa (Q-B-R) and older minerals, mark the end of vein mineralization. Chalcedonic quartz, pyrite, and marcasite appear to be nearly cogenetic, however; barite, and milky quartz were typically the latest minerals crystallized.

WALLROCK ALTERATION

Wallrock alteration was studied utilizing standard clay mineralogical X-ray diffraction (XRD) techniques, whole rock XRD, and transmitted light petrography. At various intervals within the mine a suite of samples was collected across the vein into the adjacent wallrock, typically to the tunnel margins (fig. 2). These "channel" samples were usually collected over a span of approximately 2.6 meters, which was the average width of the tunnels.

Sericite, which is a minor vein constituent, is found predominately in the wallrock directly adjacent to the veins; it occurs with fine-grained hydrothermal quartz and finely disseminated pyrite. This inner zone of Q-S-P alteration rarely extends more than 0.5 meters from the edges of the vein. Within this zone, secondary quartz in the Q-S-P altered wallrock is fine-grained, anhedral to subhedral, and light gray to gray in hand specimen. It occurs in association with sericite and finely disseminated pyrite replacing the original host rock. Both sanidine and plagioclase phenocrysts within the wallrock are altered completely to fine-grained sericite, whereas biotite phenocrysts are replaced by relatively coarse-grained, optically continuous muscovite. Hornblende phenocrysts, which are completely altered to fine-grained quartz and sericite are characteristically rimmed by leucoxene and minor fine-grained pyrite. Biotite phenocrysts also show selective alteration to leucoxene and rare fine-grained pyrite. The groundmass of the hostrock is generally altered to fine-grained quartz, sericite, and finely disseminated pyrite.

Zircon is the only primary mineral preserved within this zone.

Alteration changes laterally from Q-S-P into an assemblage containing sericite and kaolinite (S-K). Within this alteration zone, kaolinite increases away from the vein, whereas sericite content, which is greatest nearest the vein, decreases with distance from the vein. Throughout the sericite and kaolinite alteration zone, sanidine and plagioclase phenocrysts are completely altered to sericite and/or kaolinite. Biotite phenocrysts are typically replaced by muscovite, whereas fine-grained quartz and sericite occurs pseudomorphous after hornblende. Similar to the Q-S-P assemblage, leucoxene occurs after biotite and hornblende. In addition, pyrite is sparsely disseminated throughout the groundmass.

As the alteration further diminishes peripheral to the sericite-kaolinite (S-K) zone, feldspar phenocrysts are only weakly altered to sericite and/or kaolinite. In this zone, where feldspars are only weakly altered, biotite is replaced by fine-grained sericite rather than coarse-grained, optically continuous muscovite as that which occurred closer to the vein. Apatite as well as zircon are unaltered within this zone of peripheral alteration. Similar to the more intensely altered rocks, hornblende is altered to quartz, sericite, and minor amounts of fine pyrite and leucoxene. Where the Gladiator vein is exposed at the surface, the entire sequence of vein related alteration spans over a distance of 1-3 meters from the vein margins; beyond that distance, regionally altered country-rock predominates.

FLUID INCLUSION DATA

A few reconnaissance measurements of homogenization temperatures in primary fluid inclusions were made by R.F. Sanford (unpublished data). The measured fluid inclusions were in stage I (Q-S-P) quartz having primary growth bands of sericite and fluid inclusions. Six fluid inclusions from two samples taken from the "David vein" were selected. The homogenization temperatures ranged from 189.9 to 224.5°C and had a mean of 208°C and a standard deviation of 15°C. These temperatures are comparable to but near the low end of the range reported by Slack (1980) for fluid inclusions from the Ute-Ulay Mine. They are also at the low end of the range of temperatures found in other deposits in the Lake City area (R.F. Sanford, unpublished data). Measurements of freezing point of depression have not been made.

GEOCHEMICAL ANALYSIS

Eighteen vein and wall rock samples collected from the main level of the Gladiator mine (fig. 2) were analyzed for 65 elements (tables 2-6). Several techniques were utilized in these analyses; these include ICP, AA, XRF, and DNA (Sanford and others, 1987), and a new semiquantitative method as described by Sanford and Seeley (1987). The majority of the elemental anomalies correlae with specific hydrothermal vein and alteration minerals as well as primary minerals preserved in the host rock (see section on vein mineralogy). Four vein samples contain anomalous concentrations of silver (Ag) ranging from 70-500 ppm (ICP data, Table 5); two of these samples, 90 HA and 90D1B, also have proportionally high levels of antimony (Sb) (1000ppm) and to a lesser extent arsenic (As) (700-1000ppm). Petrographic and semiquantitative microprobe studies suggest that these relatively high concentrations of Ag, Sb, and As are related to tetrahedrite and Ag-bearing tetrahedrite.

In contrast, sample 90D1B, which contains 300 ppm Ag (Table 5;, Sanford and Seeley, 1987), contains only 100ppm Sb and As, significantly less As than the other three samples. Therefore, due to the low (Sb,As):Ag ratios and the lack of direct correlation between Ag and other elements found commonly as constituents in Ag-bearing minerals, it is postulated that acanthite is the Ag-bearing mineral in sample 90-D1B, although acanthite was not observed petrographically in this sample (acanthite and tetrahedrite are the only Ag-bearing minerals found in the Gladiator mine). Interestingly enough, of the samples analyzed by Seeley's method, sample 90D1B was unique of the Ag-bearing samples in that it contained anomalous Tl concentrations.

Gold (Au) was detected in 4 of the samples analyzed by Seeley's method (Table 5), and of these four samples gold content ranges from 1-10 ppm. Tellurium (Te) contents were also determined by Seeley's method. Although these samples are relatively enriched in Te (30-150 ppm), there is no apparent correlation between higher concentrations of Au and elevated levels of Te. No Au-bearing phases were identified petrographically or by microprobe analysis.

Two samples (90IA and 90IB) with over 100 ppm cadmium (Cd), as determined by ICP analysis (Table 2), also contain >10,000 ppm zinc (Zn) (ICP). It is likely that Cd, which is known to substitute for Zn is directly associated with sphalerite, the only Zn-bearing mineral occurring in the Gladiator mine. In addition, both these samples also show close correlations between anomalous bismuth (Bi), Zn, and Cd; however, it is not clear what if any significance there is in this association.

SUMMARY

A fissure-filling epithermal vein exposed in the Gladiator Mine is characterized by common base metal and gangue minerals. Silver, which is the most abundant precious metal in the vein, occurring in concentrations up to 500 ppm in selected samples, is present in tetrahedrite and rare acanthite. Three main stages of mineralization were discerned in the vein exposed in the Gladiator mine. From oldest to youngest these include: I quartz-sericite-pyrite; IIa sphalerite-galena, IIb Cu-sulfide; IIIa quartz-barite-rhodochrosite, and IIIb late barite-quartz. In general, each of these assemblages is paragenetically distinct; however, some overlapping of individual minerals within assemblages is common. Six primary fluid inclusions from stage I quartz were measured by R.F. Sanford (unpublished data). Homogenization temperatures ranged from 189.6-224.5°C and averaged 208°C. These temperatures are at the low end of the range for fluid inclusions from the Lake City area.

ACKNOWLEDGMENTS

I would like to express my gratitude to Neil Fishman, Ben Leonard, Ann Kramer, Joe Zumudio, and Rick Sanford all of the U.S. Geological Survey for their very patient assistance during the course of this study. In addition, I am indebted to Rick Sanford for the use of his fluid inclusion data.

REFERENCES

Bove, D.J., 1984, Geology and hydrothermal alteration of the Red Mountain Alunite deposit, Lake City, Colorado: Geological Society of America Abstracts with Programs, Rocky Mountain Section, v. 16, p. 216.

Bove, Dana J., 1987, Evolution of the Red Mountain alunite deposit, Lake City caldera, Colorado: U.S. Geological Survey Circular 995, Research on Mineral Resources-Programs with Abstracts, Third annual Mckelvey Forum-1987, p. 6-7.

Burbank, W.S., 1947, Lake City area, Hinsdale County, in Vanderwilt, J.W. , ed., Mineral Resources of Colorado, Denver Mineral Resources Board, p. 439-443.

Grauch, R.I., Hon, Ken, Reynolds, R.L., Bove, D.J., and Grauch, V.J.S., 1985, Episodic metallization in the western San Juan caldera complex, Colorado [abs.]: U.S. Geological Survey Circular 949, p. 14-15.

Grauch, V.J.S., 1985, Aeromagnetic and gravity models of the pluton below the Lake City caldera, Colorado [abs.]: U.S. Geological Survey Circular 949, p. 15-16.

Grauch, V.J.S. and Campbell, D.L., 1985, Gravity survey data and a Bouguer gravity anomaly map of the Lake City caldera area, Hinsdale County, Colorado: U.S. Geological Survey Open-File Report 85-208.

Grauch, V.J.S. and Hudson, M.R., 1987, Summary of natural remanent magnetization, magnetic susceptibility, and density measurements from the Lake City caldera area, San Juan Mountains, Colorado: U.S. Geological Survey Open-File Report 87-182.

Hon, Ken, Ludwig, K.R., Simmons, K.R., Slack, J.R., and Grauch, R.I., 1985, U-Pb isochron age and Pb-isotope systematics of the Golden Fleece vein--Implications for the relationship of mineralization to the Lake City caldera, western San Juan Mountains, Colorado: Economic Geology, v. 80, p. 410-418.

Hon, Ken, and Mehnert, H.H., 1983, Compilation of revised ages of volcanic units in the San Juan Mountains, Colorado: Recalculated K-Ar age determinations using IUGS constants: U.S. Geological Survey Open-File Report 83-668, 14 p.

Irving, J.D., and Bancroft, Howland, 1911, Geology and ore deposits near Lake City, Colorado: U.S. Geological Survey Bulletin 478, 128 p.

Kirk, A.R., Billings, Patty, Bove, Dana, and Sanford, R.F., 1983, Geologic Map of the Gladiator Mine, Lake City, Colorado: U.S. Geological Survey Open-File Report 83-704.

Lipman, P.W., 1976a, Caldera-collapse breccias in the western San Juan Mountains, Colorado: Geological Society of America Bulletin, v. 87, p. 1397-1410.

_____1976b, Geologic map of the Lake City caldera area, western San Juan Mountains, southwestern Colorado: U.S. Geological Survey Miscellaneous Investigations Series Map I-962.

Lipman, P.W., Fisher, F.S., Mehnert, H.H., Naeser, C.W., Luedke, R.G., and Steven, T.A., 1976, Multiple ages of mineralization and alteration in the western San Juan Mountains, Colorado: Economic Geology, v. 71, p. 571-588.

Lipman, P.W., Steven, T.A., Luedke, R.G., and Burbank, W.S., 1973, Revised volcanic history of the San Juan, Uncompahgre, Silverton, and Lake City calderas in the western San Juan Mountains, Colorado: U.S. Geological Survey Journal of Research, v. 1, p. 627-642.

Reynolds, R.L., Hudson, M.R., and Hon, Ken, 1983, Paleomagnetic evidence regarding the eruptive and resurgent history of the Lake City Caldera, San Juan Mountains, Colorado [abs.]: EOS, v. 64, p. 880.

_____1986, Paleomagnetic evidence for the timing of collapse and resurgence of the Lake City caldera, San Juan Mountains, Colorado: Journal of Geophysical Research, v. 91, no. B9, p. 9599-9613.

Sanford, R.F.,1987, Geochemistry of precious-and base-metal veins, Lake City, Colorado: U.S. Geological Survey Circular 995, p. 60-61.

Sanford, R.F., Korzeb, S.L., Seeley, J.L., and Zamudio, J.A., 1987, Geochemical data for Mineralized rocks in the Lake City Area, San Juan Volcanic Field, Southwest Colorado: U.S. Geological Survey Open-File Report 87-54.

Sanford, R.F., and Ludwig, 1985, Lead isotopic evidence on the origin of hydrothermal veins, Lake City, Colorado: Orlando GSA Abstracts with Programs, v. 17, p. 706.

Sanford, R.F. and Seeley, 1987, A new method of analysis for trace elements in gold-silver deposits: Comparison with Lake City data: U.S. Geological Survey Open-File Report 87-67.

Slack, J.F., 1976, Hypogene zoning and multistage vein mineralization in the Lake City area, western San Juan Mountains, Colorado: Stanford, California, Stanford University Ph.D. thesis, 327 p.

_____1980, Multistage vein ores of the Lake City district, western San Juan Mountains, Colorado: Economic Geology, v. 75, p. 963-991.

Srodon, Jan, and Eberl, D.D., 1984, Illite, in Ribbe, P.H., ed., Reviews in Mineralogy (Micas, v. 13): Mineralogical Society of America, p. 434-539.

Steven, T.A., and Lipman, P.W., 1976, Calderas of the San Juan volcanic field, southwestern Colorado: U.S. Geological Survey Professional Paper 958, 35 p.

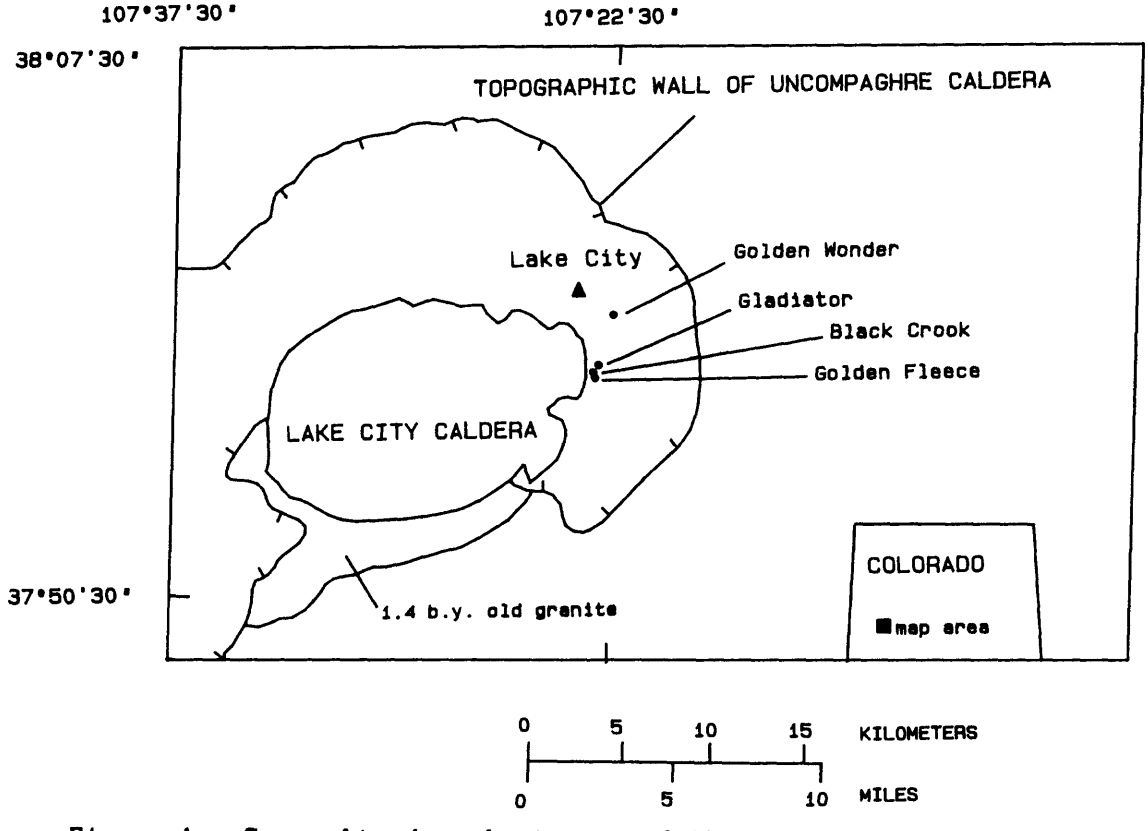

Figure 1.--Generalized geologic map of the Lake City area, showing the location of some of the more prominent mines in Lake Mining district. Modified from Lipman (1976b) and Slack (1980).

Figure 2.--Generalized geologic map of the Gladiator Mine, Lake City, Colorado. Modified from Kirk and others (1983).

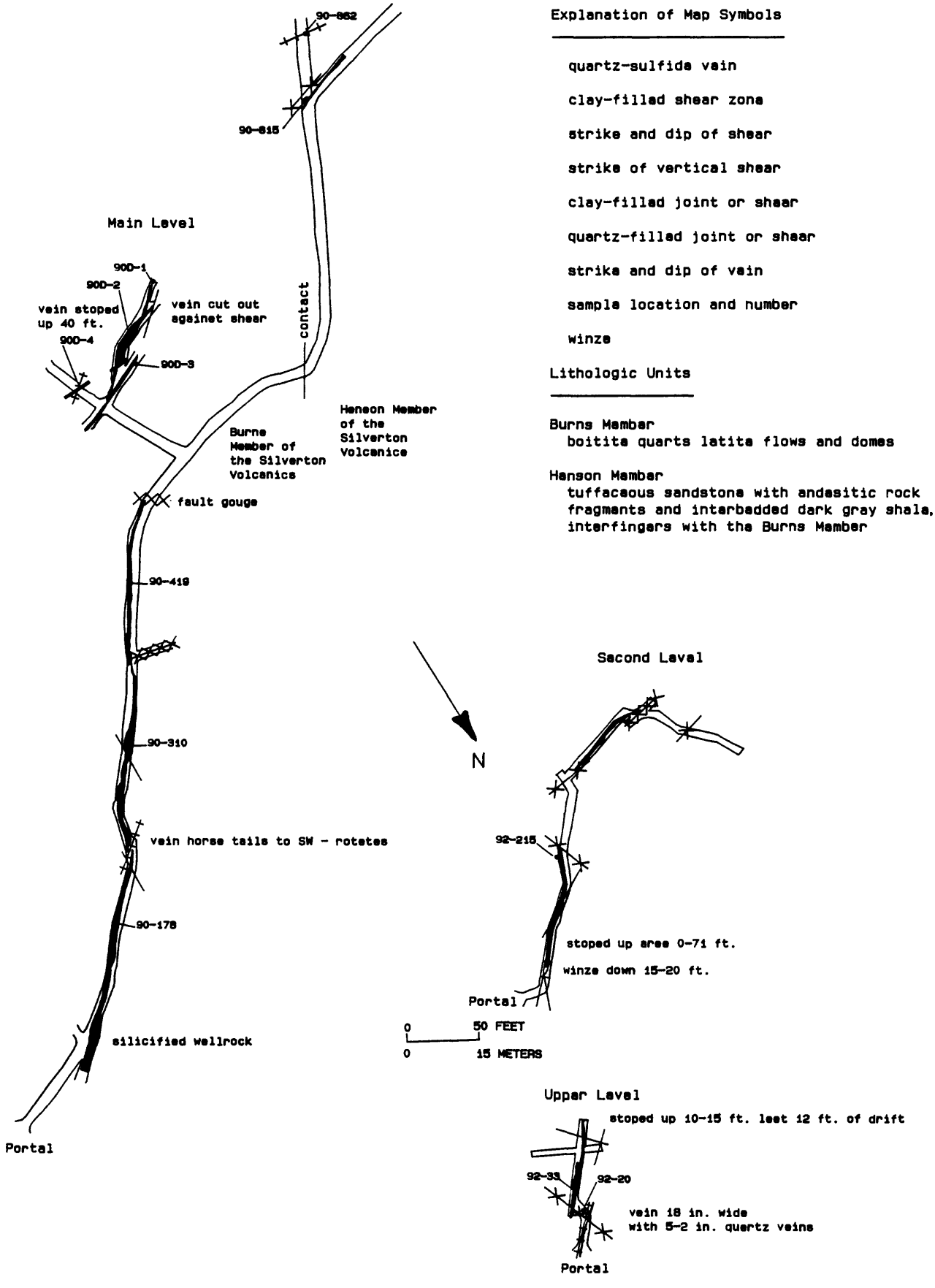

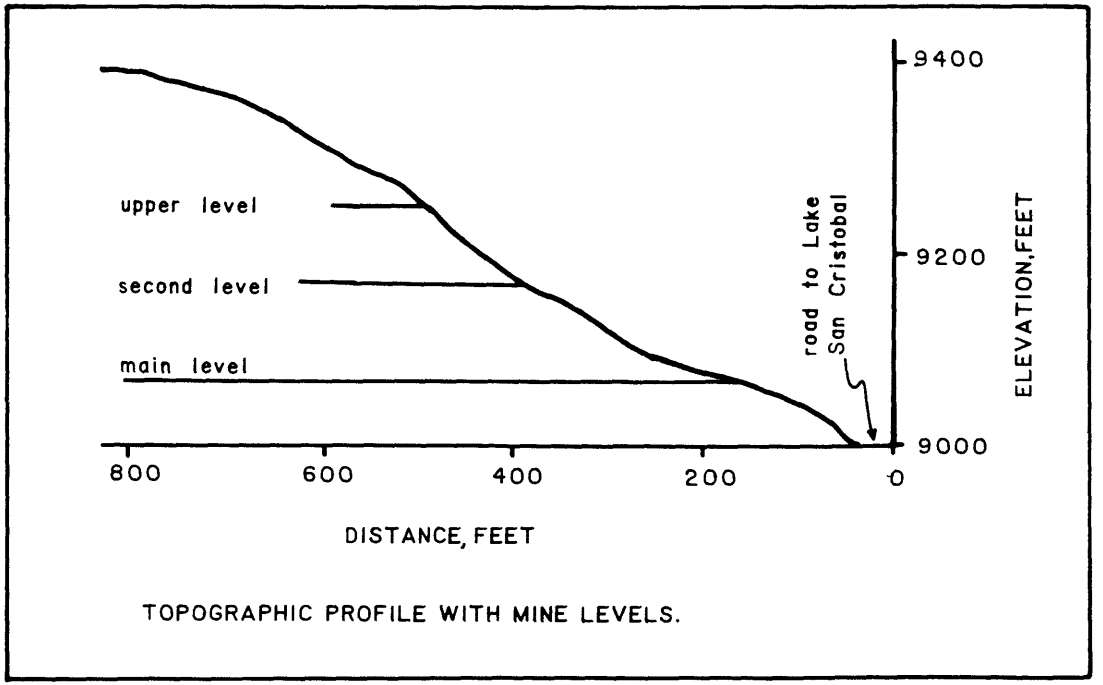

Figure 3.--Topographic profile showing the three working levels of Gladiator Mine.

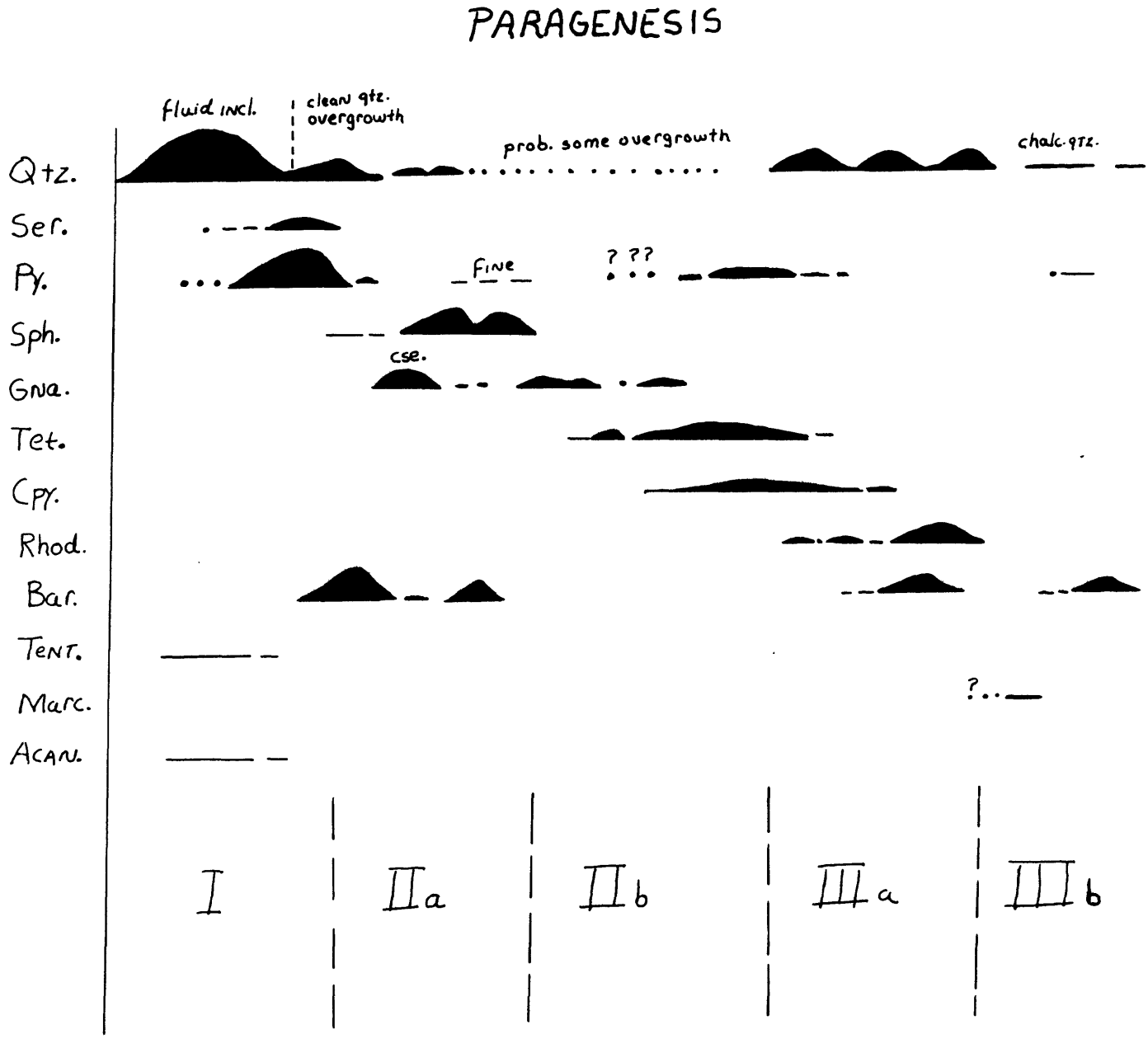

Figure 4.--Diagram depicting the paragenesis of vein minerals occurring in the Gladiator Mine.

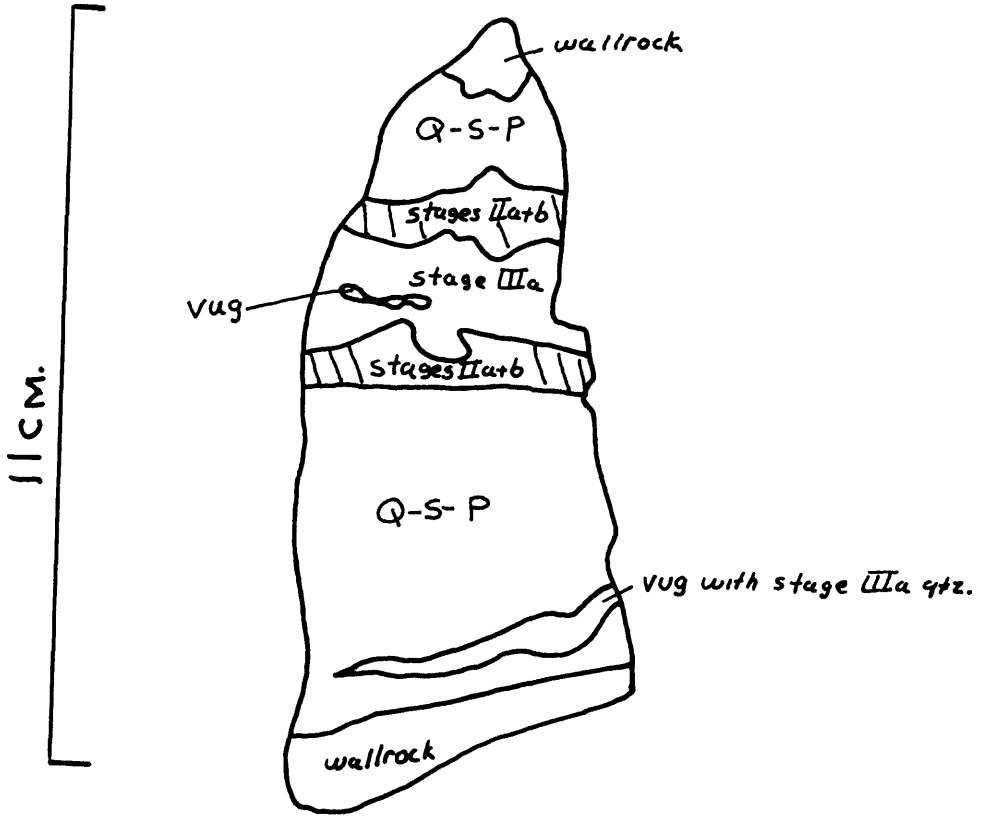

Figure 5.--Overlay sketch of hand sample from the Gladiator vein. The mineral stages are crudely banded and formed from the fissure walls inward.

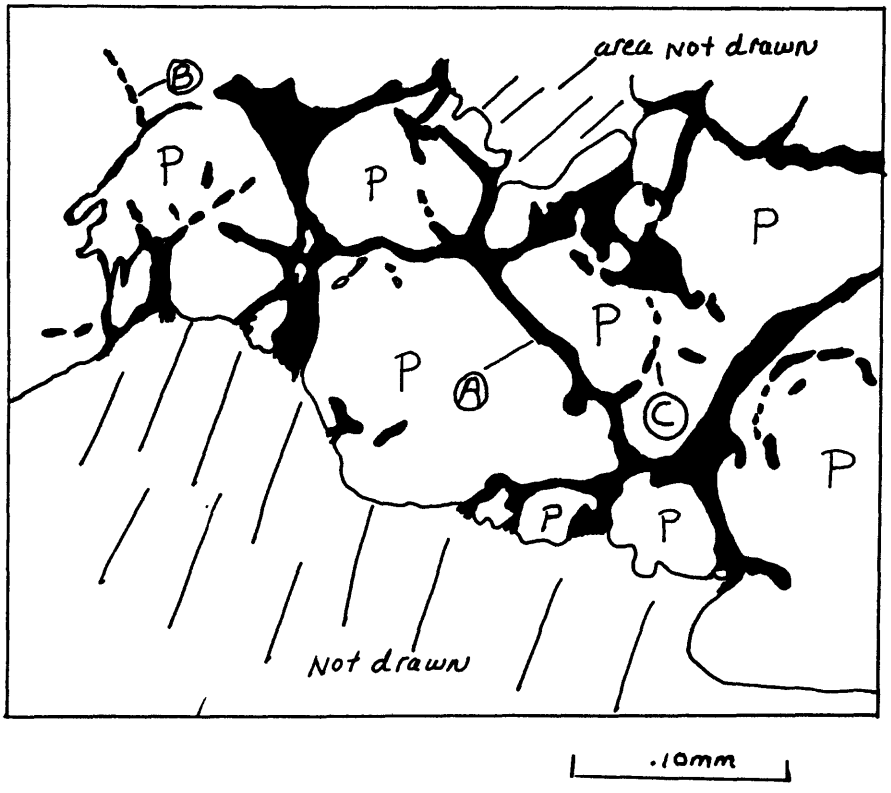

Figure 6.--Planes in stage I (Q-S-P) pyrite delineating fractures, grain margins, and zone boundaries. The sulfides along these planes are composed of tetrahedrite, sphalerite, and galena. Plane A is continuous and delineates fractures, grain margins, and overgrowth boundaries. Plane B is discontinuous however; the discontinuous planes commonly link with continuous planes, plane C.

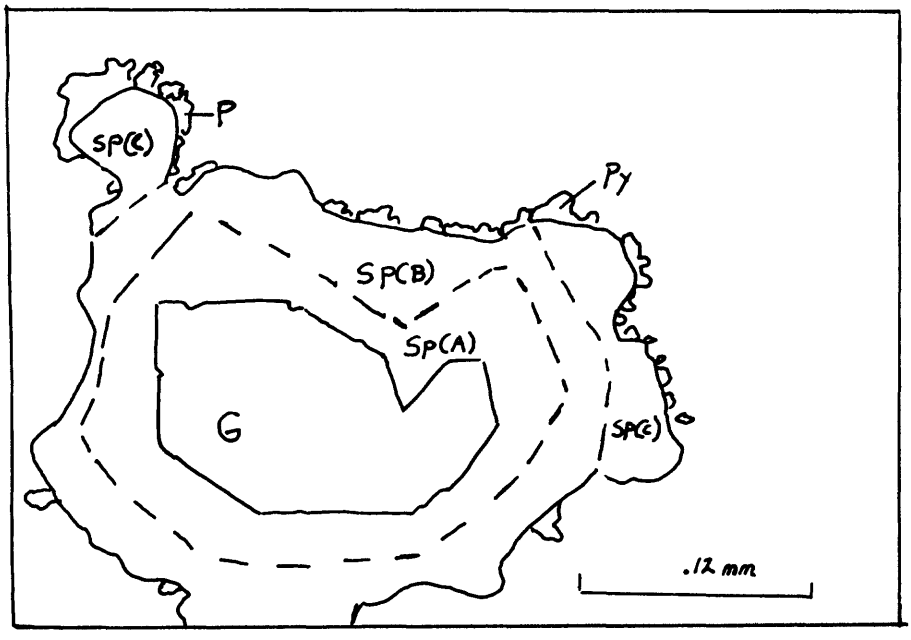

Figure 7.--Early generations of stage IIa (S-G) galena surrounded by successive bands of sphalerite (stage IIa). Stage IIb pyrite (py) grains encrust sphalerite. (A, B, and C) denote successively older generations of sphalerite.

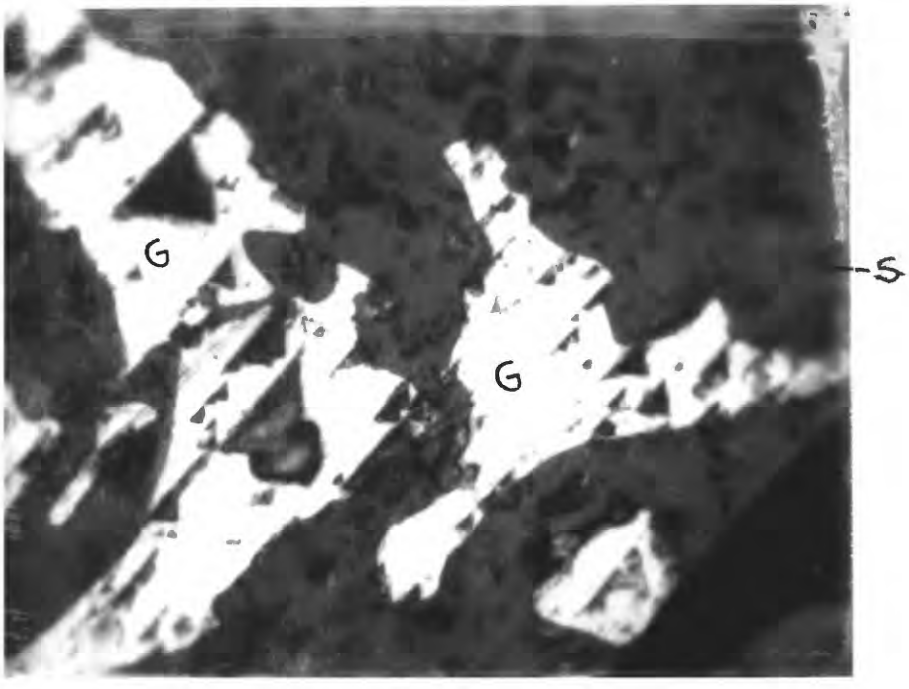

Figure 8.--Early generation of stage IIa (S-G) galena replaced by stage IIa (S-G) sphalerite.

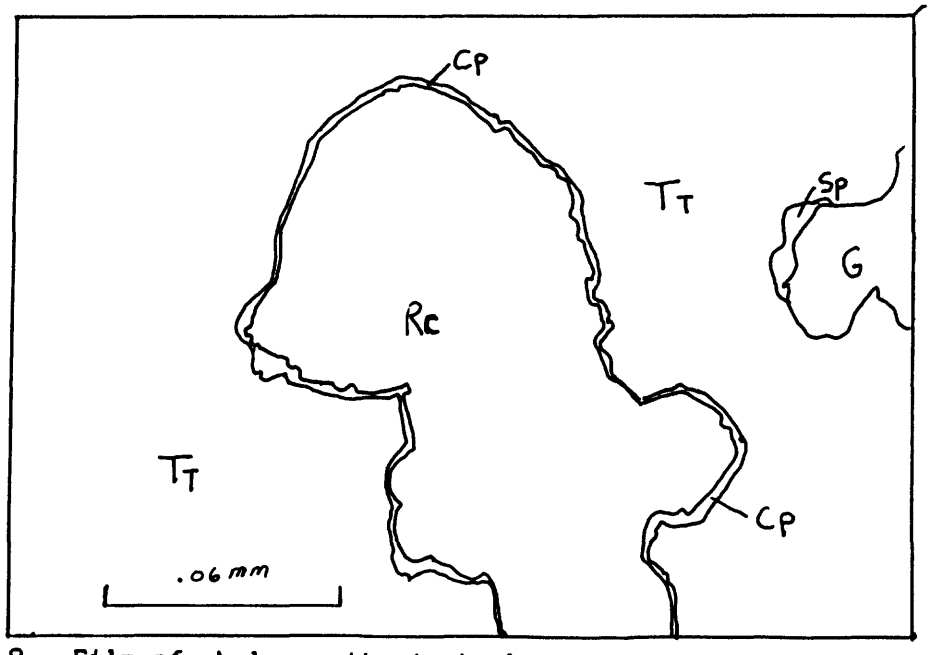

Figure 9.--Film of chalcopyrite (cp) along grain margins between tetrahedrite (Tt) and rhodochrosite (Rc). Sphalerite=(Sp), galena=(G).

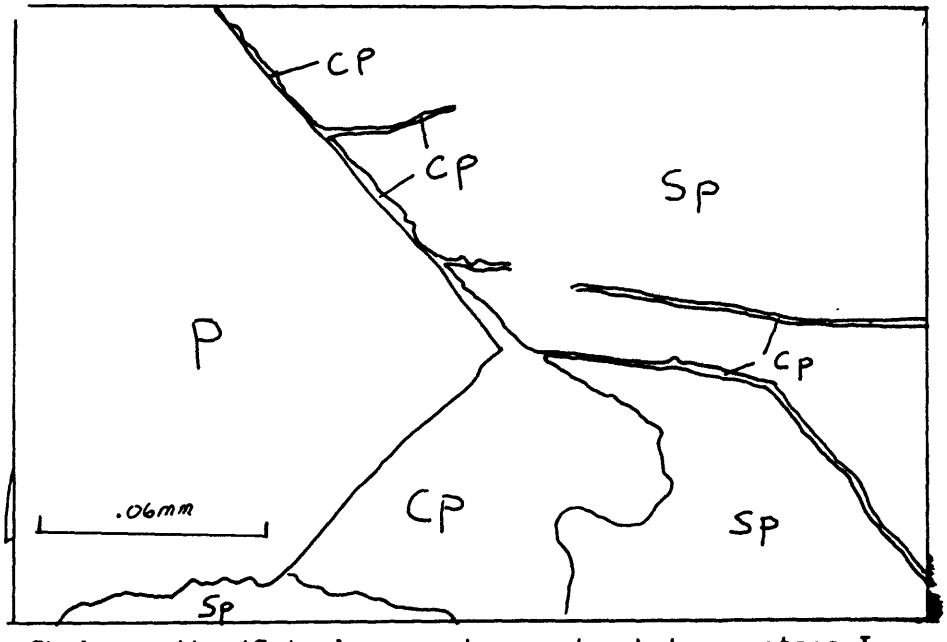

Figure 10.--Chalcopyrite (Cp) along grain margins between stage I pyrite (P) and stage IIa sphalerite (Sp) connecting with chalcopyrite-filled fractures in sphalerite.

Table 1.--Vein stages and component mineralogy

MINERAL STAGE	MAJOR MINERALS	MINOR MINERALS
I (Q-S-P)	Quartz, pyrite, sericite	Tennantite, tetrahedrite acanthite
IIa (S-G)	Sphalerite, galena, quartz, barite	Pyrite
IIb (Cu-S)	Chalcopyrite, tetrahedrite, (Ag-bearing tetrahedrite)	Galena
IIIa (Q-B-R)	Quartz, barite, rhodochrosite	Chalcopyrite
IIIb (LB-Q)	Chalcedonic quartz, barite, quartz	Pyrite, marcasite

Table 2.--USGS analyses of rocks for 42 elements by ICAP-AES (Inductively coupled argon plasma atomic emission spectroscopy, Sanford and others, 1987)

Sample	Location	Ag (ppm)	Al (percent)	As (ppm)	Au (ppm)	Ba (ppm)	Be (ppm)	Bi (ppm)	Ca (percent)	Cd (ppm)	Ce (ppm)	Co (ppm)	Cr (ppm)	Cu (ppm)
2K90C11H	61	---	8.70	<20	<20	---	<2	<20	2.00	<4	110	12	9	14
2K90C18H	61	---	2.80	80	<20	---	3	<20	<.01	42	18	<2	3	810
2K90C32H	61	---	6.20	60	<20	---	<2	<20	.08	<4	28	4	4	14
2K90C42H	61	---	6.10	<20	<20	---	2	<20	.37	<4	67	3	5	270
2K90C52H	61	---	7.20	<20	<20	---	2	<20	.09	<4	100	4	5	52
2K90D1AH	61	---	11.00	60	<20	---	2	<20	.21	<4	160	5	7	6
2K90D1BJ	61	500	.10	290	<20	>100,000	<2	240	.01	77	<8	2	<2	10,000
2K90FA H	61	---	5.70	50	<20	---	2	<20	.04	<4	45	4	4	150
2K90FB H	61	---	6.40	50	<20	---	2	<20	.05	<4	34	3	3	140
2K90FC H	61	---	8.80	130	<20	---	3	<20	.20	<4	120	5	6	81
2K90FD H	61	---	7.00	30	<20	---	2	<20	.06	6	95	4	5	740
2K90FE J	61	100	.25	1,200	<20	700	<2	<20	.02	42	<8	4	<2	640
2K90FF J	61	300	.27	620	<20	>100,000	<2	<20	.02	23	<8	3	<2	2,300
2K90FG J	61	70	.48	90	<20	15,000	<2	<20	.03	<4	<8	3	2	2,000
2K90FH H	61	---	2.50	20	<20	---	<2	<20	.04	<4	75	5	6	34
2K90HA G	61	---	.18	4,900	<20	---	<2	100	.06	300	<8	4	<2	22,000
2K90IA G	61	---	3.40	30	<20	---	<2	<20	.17	<4	28	4	2	440
2K90IB G	61	---	.14	2,400	<20	---	<2	<20	.11	290	<8	2	<2	14,000

Table 2.--USGS analyses of rocks for 42 elements by ICAP-AES--Continued

Sample	Location	Ni (ppm)	P (percent)	Pb (ppm)	Pr (ppm)	Sc (ppm)	Sn (ppm)	Sr (ppm)	Th (ppm)	Ti (percent)	U (ppm)	V (ppm)	Y (ppm)	Yb (ppm)	Zn (ppm)
2K90C11H	61	7	.13	23	<20	12	<8	---	<8	.39	<200	110	16	<2	430
2K90C18H	61	<4	<.01	2,400	<20	<4	<8	---	17	.05	<200	10	4	<2	5,200
2K90C32H	61	<4	<.01	39	<20	<4	<8	---	<8	.18	<200	29	5	<2	60
2K90C42H	61	<4	.17	28	<20	<4	<8	---	<8	.17	<200	35	8	<2	110
2K90C52H	61	<4	.01	120	<20	<4	<8	---	9	.21	<200	33	6	<2	330
2K90D1AH	61	6	.09	48	<20	5	<8	---	12	.26	<200	52	14	<2	250
2K90D1BJ	61	<4	<.01	70,000	<20	<4	<8	7,000	<8	<.01	<200	<4	<4	<2	11,000
2K90FA H	61	<4	<.01	200	<20	<4	<8	---	<8	.16	<200	42	6	<2	510
2K90FB H	61	<4	<.01	80	<20	<4	<8	---	<8	.17	<200	49	7	<2	390
2K90FC H	61	8	.06	350	<20	5	<8	---	13	.23	<200	49	11	<2	760
2K90FD H	61	5	<.01	200	<20	5	<8	---	15	.20	<200	47	8	<2	1,400
2K90FE J	61	<4	.02	100,000	<20	<4	<8	7	<8	<.01	<200	5	7	<2	8,700
2K90FF J	61	<4	<.01	1,500	<20	<4	<8	7,000	<8	<.01	<200	<4	<4	<2	250
2K90FG J	61	<4	<.01	700	<20	<4	<8	150	<8	<.01	<200	4	<4	<2	450
2K90FH H	61	<4	.02	440	<20	5	<8	---	9	.31	<200	64	7	<2	160
2K90HA G	61	<4	.02	7,300	<20	<4	<8	25	<8	<.01	<200	<4	12	<2	41,000
2K90IA G	61	5	.07	140	<20	<4	<8	21	<8	.08	<200	29	6	<2	240
2K90IB G	61	<4	<.01	13,000	<20	<4	<8	97	22	<.01	<200	<4	6	<2	42,000

Table 2.--USGS analyses of rocks for 42 elements by ICAP-AES--Continued

Sample	Location	Dy (ppm)	Er (ppm)	Eu (ppm)	FeTot (percent)	Ga (ppm)	Gd (ppm)	K (percent)	La (ppm)	Li (ppm)	Mg (percent)	Mn (ppm)	Mo (ppm)	Na (percent)	Nb (ppm)	Nd (ppm
2K90C11H	61	<8	<8	<4	3.80	18	<20	5.8	47	22	.87	1,100	<4	1.10	<8	33
2K90C18H	61	<8	<8	<4	.98	29	<20	1.1	10	47	.08	84	12	.01	11	<8
2K90C32H	61	<8	<8	<4	2.90	13	<20	2.5	12	25	.19	160	<4	.02	<8	8
2K90C42H	61	<8	<8	<4	1.80	13	<20	2.6	30	19	.26	710	<4	.03	<8	20
2K90C52H	61	<8	<8	<4	1.70	12	<20	5.4	45	17	.27	2,800	<4	.07	<8	25
2K90D1AH	61	<8	<8	<4	2.30	19	<20	7.2	66	51	.13	2,500	<4	.12	<8	39
2K90D1BJ	61	<8	<8	<4	6.50	<8	<20	<.1	<4	26	<.01	57	<4	.02	<8	<8
2K90FA H	61	<8	<8	<4	1.50	14	<20	2.7	21	24	.30	310	6	.02	<8	11
2K90FB H	61	<8	<8	<4	1.50	13	<20	3.0	17	18	.33	260	<4	.02	8	<8
2K90FC H	61	<8	<8	<4	1.90	17	<20	5.4	53	27	.39	1,200	<4	.06	<8	<34
2K90FD H	61	<8	<8	<4	2.00	18	<20	3.4	43	23	.38	240	<4	.04	11	28
2K90FE J	61	<8	<8	<4	7.60	<8	<20	<.1	6	80	.01	85	<4	.03	<8	<8
2K90FF J	61	<8	<8	<4	.60	<8	<20	<.1	<4	51	.01	26	<4	.02	<8	<8
2K90FG J	61	<8	<8	<4	.99	<8	<20	.1	<4	88	.03	330	<4	.04	<8	<8
2K90FH H	61	<8	<8	<4	1.30	8	<20	.9	30	73	.04	53	<4	.03	<8	20
2K90HA G	61	<8	<8	<4	16.00	<8	<20	<.1	<4	35	.01	10,000	<4	.02	<8	<8
2K90IA G	61	<8	<8	<4	1.60	11	<20	1.5	17	42	.17	260	<4	.03	<8	14
2K90IB G	61	<8	<8	<4	7.30	<8	<20	<.1	4	40	.08	90,000	<4	.02	<8	<8

Table 3.--USGS analyses of rocks for "major elements" by X-ray fluorescence

Sample	Location	SiO_2 (percent)	TiO_2 (percent)	Al_2O_3 (percent)	T-Fe_2O_3 (percent)	MnO (percent)	MgO (percent)	CaO (percent)	Na_2O (percent)	K_2O (percent)	P_2O_5 (percent)	LOI (900°C)
2K90C11H	61	59.4	.69	16.00	5.31	.14	1.47	2.91	1.21	7.17	.31	4.00
2K90C18H	61	87.1	.07	5.32	1.33	<.02	.19	<.02	<.15	1.32	<.05	2.26
2K90C32H	61	74.7	.32	11.80	4.12	<.02	.38	.08	<.15	3.21	<.05	4.15
2K90C42H	61	76.1	.32	11.40	2.50	.09	.50	.54	<.15	3.27	.40	3.22
2K90C52H	61	71.9	.37	13.60	2.22	.37	.51	.10	<.15	6.92	<.05	2.79
2K90D1AH	61	70.2	.38	14.40	2.34	.23	.22	.19	<.15	6.57	.15	3.94
2K90FA H	61	78.7	.27	10.70	1.89	.03	.56	.03	<.15	3.37	<.05	2.74
2K90FB H	61	74.2	.33	13.10	2.38	.03	.65	.05	<.15	4.16	<.05	2.97
2K90FC H	61	70.2	.39	14.70	2.39	.13	.64	.23	<.15	6.05	.14	3.47
2K90FD H	61	74.2	.38	13.10	2.74	.02	.70	.06	<.15	4.31	<.05	3.07
2K90FH H	61	88.5	.65	4.75	1.75	<.02	.12	.03	<.15	1.13	.07	1.80

Table 4.--USGS analyses of rocks for 10 elements by supplemental techniques (Various single element techniques; see Sanford and others, 1987)

Sample	Location	CO_2 (percent)	F (percent)	FeO (percent)	H_2O^+ (percent)	H_2O^- (percent)	Hg (ppm)	T-S (percent)	S (percent)	SO_3 (percent)	Sb (ppm)
2K90D1BJ	61	---	---	---	---	---	---	14.00	---	.25	1,100
2K90FA H	61	<.01	---	---	1.57	.23	---	1.07	.50	---	---
2K90FB H	61	<.01	---	---	1.85	.23	---	1.16	.56	---	---
2K90FC H	61	.18	---	---	2.33	.22	---	1.04	.62	---	---
2K90FD H	61	<.01	---	---	1.93	.23	---	1.18	.71	---	---
2K90FE J	61	---	---	---	---	---	---	---	---	---	180
2K90FF J	61	---	---	---	---	---	---	---	---	---	1,700
2K90FG J	61	---	---	---	---	---	---	---	---	---	310
2K90HA G	61	---	---	---	---	---	4.00	22.20	---	.08	3,400
2K90IA G	61	---	---	---	---	---	.05	1.69	---	<.03	170
2K90IB G	61	---	---	---	---	---	1.50	10.20	---	.23	3,100

Table 5.--USGS analyses of rocks for 11 elements by Seeley modification of semiquantitative emission spectroscopic 6-step) method (Sanford and Seeley, 1986)

Sample	Location	Ag	As	Au	Bi	Ga	Hg	In	Sb	Sn	Te	Tl
2K90D1BJ	33	300.0	100	2.0	100.0	1.0	5.0	2.0	100	---	30	>100.0
2K90FG J	33	30.0	500	.2	3.0	1.0	5.0	2.0	500	3	150	<.3
2K90HA G	33	500.0	1,000	2.0	70.0	.5	5.0	100.0	1,000	10	100	<.3
2K90IA G	33	200.0	700	.2	5.0	<.5	3.0	100.0	1,000	10	50	<.3

Table 6.--USGS analyses of rocks for uranium and thorium by delayed neutron activation

Sample	Location	U (ppm)	Th (ppm)
2K90C11H	61	2.410	14.80
2K90C18H	61	4.670	30.30
2K90C32H	61	6.240	15.70
2K90C42H	61	5.560	12.90
2K90C52H	61	5.680	18.60
2K90D1AH	61	5.350	22.60
2K90D1BJ	61	1.770	6.17
2K90FA H	61	4.840	14.20
2K90FB H	61	5.450	15.50
2K90FC H	61	5.020	20.10
2K90FD H	61	6.040	19.00
2K90FE J	61	31.500	<2.80
2K90FF J	61	1.460	<1.10
2K90FG J	61	8.420	<3.10
2K90FH H	61	11.800	17.00
2K90HA G	61	3.730	<1.80
2K90IA G	61	11.100	<3.80
2K90IB G	61	.317	<.83